The Astrophysical Journal Letters, 934:L22 (8pp), 2022 August 1 https://doi.org/10.3847/2041-8213/ac8169

Spectral Analysis of GRB 220426A: Another Case of a Thermally Dominated Burst

Li-Tao Deng[1], Da-Bin Lin[1], Li Zhou[1], Kai Wang[1], Xing Yang[1], Shu-Jin Hou[1,2], Jing Li[1], Xiang-Gao Wang[1], Rui-Jing Lu[1], and En-Wei Liang[1]
[1] Laboratory for Relativistic Astrophysics, Department of Physics, Guangxi University, Nanning 530004, People's Republic of China; lindabin@gxu.edu.cn
[2] College of Physics and Electronic Engineering, Nanyang Normal University, Nanyang, Henan 473061, People's Republic of China; houshujingrb@163.com
Received 2022 May 17; revised 2022 July 12; accepted 2022 July 15; published 2022 July 28

Abstract

We report a very bright, long-duration gamma-ray burst (GRB), GRB 220426A, observed by the Fermi satellite. GRB 220426A, with a total duration of $T_{90} = 6$ s, is composed of two main pulses and some subpeaks. The spectral analysis of this burst with a Band function reveals that both the time-integrated and the time-resolved spectra are very narrow with a high $\alpha \gtrsim 0.2$ and low $\beta \lesssim -3.1$. It is highly reminiscent of GRB 090902B, a special GRB with a photospheric emission identification. Then, we perform the spectral analysis of this burst based on nondissipated photospheric emission, which can be well modeled by a multicolor blackbody with a cutoff power-law distribution of the thermal temperature. The spectral fittings reveal that the photospheric emission can well describe the radiation spectrum of this burst. We conclude that this burst would be a second burst in the class of GRB 090902B observed by the Fermi satellite. We also discuss the physics of the photosphere and the origin of the high-energy component in GRB 220426A.

Unified Astronomy Thesaurus concepts: Gamma-ray bursts (629)

1. Introduction

The emission mechanism of gamma-ray bursts (GRBs) has been a puzzle since their discovery half a century ago. The difficulty in understanding prompt emission mainly lies in the fact that no known theoretical models can straightforwardly interpret all of the observational data. According to the large statistics of the temporal and spectral properties of the prompt emission, two main categories of the prompt emission mechanism are proposed. One invokes the nonthermal emission mechanism, owing to the nonthermal characteristic of the Band component observed in most GRBs. In this scenario, previous works have shown that the synchrotron or synchrotron self-Compton radiation emitted by accelerated electrons is a promising mechanism (Tavani 1996; Lloyd & Petrosian 2000; Zhang & Mészáros 2002; Daigne et al. 2011; Zhang & Yan 2011; Uhm & Zhang 2014). Another mechanism is the Comptonized quasi-thermal emission from the outflow photosphere (Thompson 1994; Ghisellini & Celotti 1999; Pe'er et al. 2006; Thompson et al. 2007; Giannios 2008; Lazzati & Begelman 2010; Mizuta et al. 2011; Lazzati et al. 2013; Ruffini et al. 2013), according to the quasi-thermal components detected in the spectrum of some GRBs (Ryde 2004; Ryde 2005; Ryde & Pe'er 2009; Abdo et al. 2009; Ryde et al. 2010; Zhang et al. 2011; Guiriec et al. 2011; Toma et al. 2011; Axelsson et al. 2012; Ghirlanda et al. 2013; Guiriec et al. 2013; Larsson et al. 2015). Although thermal components are rarely observed, their contributions to the GRB prompt emission could not be ignored. In the classical fireball scenario, photospheric emission is suggested to be an obvious component in the prompt emission (Mészáros & Rees 2000; Mészáros et al. 2002; Daigne & Mochkovitch 2002; Rees & Mészáros 2005). For a burst with low or intermediate magnetization in the jet composition, the photospheric emission may appear as a shoulder in the radiation spectrum of the prompt emission (e.g., Gao & Zhang 2015; Beniamini & Giannios 2017). Observationally, bright photospheric emission is indeed found in several bursts, e.g., GRB 090902B, which highlights the importance of the photospheric emission during the GRB prompt phase.

GRB 090902B is a bright, long GRB, detected by the Gamma-ray Burst Monitor (GBM) and Large Area Telescope on board the Fermi Gamma-ray Space Telescope. The spectrum of its prompt emission is peculiar. Some works revealed that the gamma-ray prompt emission of this burst is dominated by thermal emission in the energy range from ∼50 keV to ∼10 MeV (Abdo et al. 2009; Ryde et al. 2010; Zhang et al. 2011). Abdo et al. (2009) revealed that both the time-integrated and time-resolved spectra of this burst can be fitted with the Band function and an additional power-law spectral component. Compared with the Band component found in other GRBs, however, the Band component in GRB 090902B is very narrow, with $\alpha \sim -0.3$ and $\beta \sim -3.32$, rather than the general values of $\alpha \sim -1$ and $\beta \sim -2.3$ (Preece et al. 2000). Because the shape of the Band component in this burst is too narrow for synchrotron radiation, it is likely of a photospheric origin. Based on the spectral model of a multicolor blackbody with a power-law distribution of temperatures, Ryde et al. (2010) found that the time-resolved spectra of the prompt emission in this burst can be well fitted. GRB 220426A is a bright burst with a duration of $T_{90} \sim 6$ s over the energy range from 50 keV to 300 keV. In the period of [0.002, 9.856] s after the Fermi trigger, the fluence in the energy range of 10–1000 keV is $(1.084 \pm 0.005) \times 10^{-4}$ erg cm^{-2} and the time-integrated spectrum fitted by a Band function reports a narrow Band component with $E_{\rm p} = 146.3 \pm 0.9$ keV, $\alpha = -0.05 \pm 0.01$, and $\beta = -3.08 \pm 0.04$ (Malacaria et al. 2022). This burst also triggered the observation of the Konus-Wind experiment (Frederiks et al. 2022). Based on the Konus-Wind observation, the time-integrated spectral analysis of this burst also reveals a narrow Band component with $\alpha = -0.29^{+0.07}_{-0.07}$ and $\beta = -4.00^{+0.32}_{-0.71}$ in this burst (Frederiks et al. 2022). The narrow Band component found in this burst is very similar to that found in GRB 090902B. Thus, we would like to believe that the photosphere emission is responsible for the prompt emission of GRB 220426A.

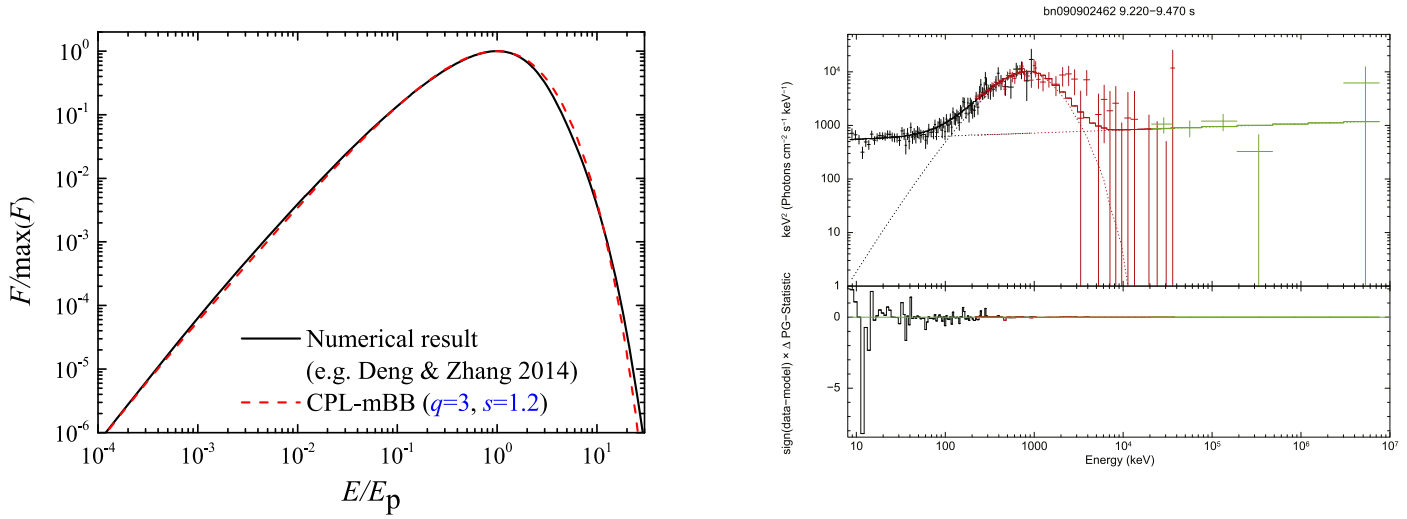

Figure 1. Left panel: modeling the radiation spectrum of photospheric emission with CPL-mBB (red dashed line), where the solid line is the numerical result (e.g., Deng & Zhang 2014). Right panel: fitting the radiation spectrum of GRB 090902B with CPL-mBB and the power-law spectral model.

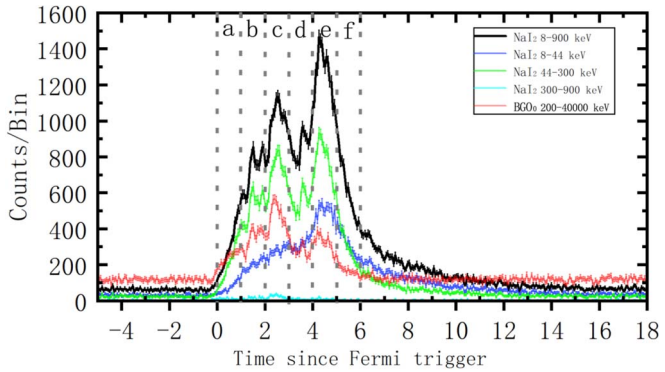

Figure 2. Light curves of GRB 220426A in different energy ranges.

In this Letter, we report on the observations and spectra analysis of GRB 220426A. The paper is organized as follows. In Section 2, the modeling of a nondissipated photosphere emission is presented. Different from Ryde et al. (2010), a multicolor blackbody emission model with a cutoff power-law distribution of temperature is proposed. In Section 3, the data reduction and the spectral analysis of GRB 220426A are performed. In Section 5, we present the conclusion and discuss this burst.

2. Spectra Modeling of a Nondissipated Photospheric Emission

Several GRBs are identified as having a distinct thermal component by fitting them with a Plank radiation spectrum. However, the photospheric emission is generally different from a single blackbody emission owing to the inherent geometric effects of the jet. For example, the observed temperature is latitude dependent due to the Doppler shift and the latitude-dependent photospheric radius (Pe'er 2008). Therefore, the photospheric emission is better represented by the emission from a multicolor blackbody (mBB) instead of a single blackbody. Ryde et al. (2010) suggest that the observed spectral flux at a photon energy E from the photospheric emission can be described with (i.e., mBB)

$$F^{\rm mBB}(E, T_{\rm max}) = \int_{T_{\rm min}}^{T_{\rm max}} \frac{dA(T)}{dT} \frac{E^3}{\exp(E/kT) - 1} dT, \quad (1)$$

where $T_{\rm max}$ is a free parameter and $T_{\rm min} \ll T_{\rm max}$ cannot be determined. For each Planck function, the spectrally integrated flux for each Planck function is given by $f(T) = A(T)(kT)^4\pi^4/15$, where $A(T)$ is the normalization as a free parameter. In Ryde et al. (2010), the contribution of each single blackbody emission is taken to be

$$f(T) = f_{\rm max}\,(T/T_{\rm max})^q\,, \quad (2)$$

where $f_{\rm max}$ is the spectrally integrated flux at $T = T_{\rm max}$ and the index q is a free parameter.

In reality, an individual photon in the jet can be scattered to an observer by an electron at any position in the outflow with a certain probability. That is to say, the observed photons can be from both the different latitude and different radius of the jet. Because the observed probability P of a photon is related to the optical depth τ for photons from their location to an observer, i.e., $P \propto \exp(-\tau)$, a power-law distribution of the temperature for the mBB may not describe well the contribution of the emission from a different radius of the jet. By fitting the radiation spectrum of the photosphere from the numerical calculation (e.g., Deng & Zhang 2014), we point out that the temperature distribution of the mBB used to describe well the photospheric emission may be

$$f(T) = f_{\rm max}\,(T/T_{\rm c})^q \exp[-(T/T_{\rm c})^s], \quad (3)$$

where $T_{\rm c}$ is the cutoff temperature. The mBB with temperature distribution as in Equation (3) or (2) is denoted as CPL-mBB or PL-mBB, respectively. In the left panel of Figure 1, one can find that the CPL-mBB with $q = 3$ and $s = 1.2$ can well model the emission of a nondissipated photosphere. Here, $T_{\rm max} \gg T_{\rm c}$ is taken in CPL-mBB, $r_{\rm ph}$ is the radius of the photosphere, and $r_{\rm s}$ is the saturation radius of the fireball. In the right panel of Figure 1, we show the time-resolved EF_E spectrum fitting of GRB 090902B with the CPL-mBB and power-law spectral model for one of the time intervals in Table 1 of Ryde et al. (2010), i.e., [9.22, 9.47] s. The value of C-stat/dof = 286.75/286 is reported in the fitting.

We would apply the CPL-mBB with $q = 3$ and $s = 1.2$ to fit the thermal component in other GRBs. Based on the fitting

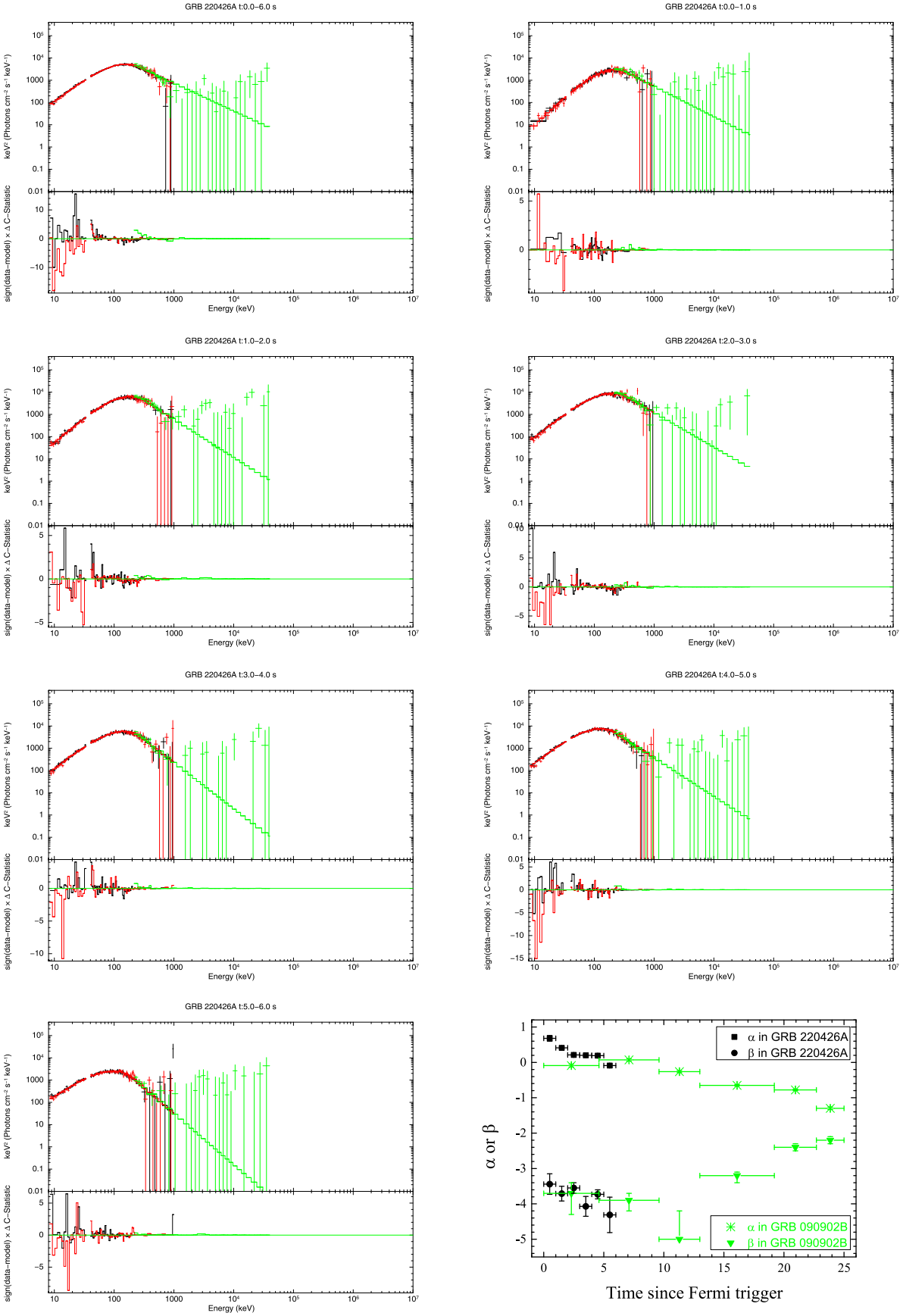

Figure 3. Spectrum analysis results of GRB 220426A with the Band function. Here, the bottom-right panel plots the evolution of α and β in this burst and GRB 090902B (from Table 1 of Abdo et al. 2009).

Table 1
Spectral Fittings of GRB 220426A with the Band Function (Columns 3–7) and CPL-mBB with $q = 3$ and $s = 1.2$ (Columns 8–10)

Time Interval	Labels	α	β	E_p(keV)	Norm	C-stat/dof	kT_c(keV)	f_{max} (keV s^{-1} cm^{-2})	C-stat/dof
[0, 6] s		0.11 ± 0.01	-3.25 ± 0.05	75.04 ± 0.94	1.67 ± 0.03	627.97/357	17.39 ± 0.06	2338 ± 9.56	707.32/359
[0, 1] s	*a*	0.68 ± 0.08	-3.44 ± 0.29	83.03 ± 4.64	0.52 ± 0.04	313.00/357	28.78 ± 0.53	1283 ± 26.83	340.49/359
[1, 2] s	*b*	0.41 ± 0.03	-3.71 ± 0.21	77.05 ± 2.05	1.60 ± 0.07	363.50/357	22.03 ± 0.20	2686 ± 28.76	358.22/359
[2, 3] s	*c*	0.21 ± 0.03	-3.55 ± 0.15	92.00 ± 2.12	1.71 ± 0.05	398.11/357	22.68 ± 0.17	3848 ± 34.02	372.51/359
[3, 4] s	*d*	0.20 ± 0.03	-4.07 ± 0.28	65.88 ± 1.62	2.28 ± 0.10	342.02/357	16.03 ± 0.13	2416 ± 22.58	322.64/359
[4, 5] s	*e*	0.19 ± 0.03	-3.73 ± 0.13	57.97 ± 1.21	4.00 ± 0.16	408.71/357	14.13 ± 0.09	3231 ± 23.90	369.14/359
[5, 6] s	*f*	-0.09 ± 0.04	-4.31 ± 0.50	50.02 ± 1.77	1.86 ± 0.14	275.67/357	9.89 ± 0.10	1107 ± 12.36	271.55/359

result with CPL-mBB, one can obtain the value of T_c and f_{max}. The photospheric temperature T_{ph} of the outflow propagating along the light of sight is related to the value of T_c by $T_{ph} = 3T_c$ according to the numerical results. Correspondingly, $F_{ph} \equiv \sigma T_{ph}^4 r_{ph}^2 \Big/ d_L^2 = 0.63 \int_0^{+\infty} F^{mBB} dE$ according to the numerical results. The values of T_{ph} and F_{ph} can be used to estimate the properties of the photosphere.

3. Data Reduction and Spectral Analysis of GRB 220426A

GRB 220426A was detected by the Fermi Gamma-Ray Burst Monitor (GBM) at 07:14:08 UT (T_0) on 2022 April 26 with a duration of $T_{90} \sim 6$ s estimated in the energy band of 50–300 keV (Malacaria et al. 2022). GBM has 12 sodium iodide (NaI) scintillation detectors covering the 8 keV–1 MeV energy band, and two bismuth germanate (BGO) scintillation detectors that are sensitive to the 200 keV–40 MeV energy band (Meegan et al. 2009). The brightest NaI and BGO detectors, i.e., NaI2 and BGO0, are used for our analyses. The light curve of GRB 220426A can be found in Figure 2. From these light curves, one can find that the burst consists of double main pulses with some subpeaks.

As reported by Biltzinger et al. (2022), the time-averaged spectrum from 0.002 s to 9.856 s can be fitted with the Band function and the best-fit result of the Band function is $E_p = 146.3 \pm 0.9$ keV, $\alpha = -0.05 \pm 0.01$, and $\beta = -3.08 \pm 0.04$. It reveals that the Band component in this burst is very narrow. Then, we would like to perform a detailed spectral analysis of the prompt emission in this burst. First, the Band function is used in our spectral fitting. The fitting results can be found in Figure 3 and reported in columns 3–7 of Table 1, where different time intervals, i.e., [0, 6] s, [0, 1] s, [1, 2] s, [2, 3] s, [3, 4] s, [4, 5] s, and [5, 6] s, are adopted. Here, the time intervals of [0, 1] s, [1, 2] s, [2, 3] s, [3, 4] s, [4, 5] s, and [5, 6] s are indicated in Figure 2 with labels a, b, c, d, e, and f, respectively. In the time interval [0, 6] s, the best-fitting result with the Band function reports $E_0 = 75.04 \pm 0.94$ keV, $\alpha = 0.11 \pm 0.01$, and $\beta = -3.25 \pm 0.05$, which is consistent with the result reported in Biltzinger et al. (2022). In the other time intervals, the spectral fittings also reveal a narrow Band component with a high value of $\alpha \sim 0.3$ and a low value of $\beta \sim -3.4$. Both high α and low β are highly reminiscent of GRB 090902B, the spectral analysis of which with the Band function reported $\alpha \gtrsim -0.3$ and $\beta \lesssim -3.7$ in the time intervals of [0, 13] s after the Fermi trigger.

The narrow Band component of GRB 090902B is found to be consistent with a multicolor quasi-thermal spectrum (Ryde et al. 2010; Zhang et al. 2011). In the bottom-right panel of Figure 3, we plot the evolution of α and β with time for GRB 220426A and GRB 090902B in their prompt emission phase, where the values of α and β are taken from Table 1 of Abdo et al. (2009). One can find that the values of α in GRB 220426A are generally higher than those in GRB 090902B although the values of β for these two bursts are almost the same. This implies that the radiation spectra of the prompt emission in GRB 220426A are narrower than those in GRB 090902B. Then, we would like to believe that the narrow Band component found in GRB 220426A may be also consistent with a multicolor quasi-thermal spectrum. In Figure 4, we show the spectral fitting results of GRB 220426A with CPL-mBB, $q = 3$, and $s = 1.2$. The fitting results are also reported in columns 8–10 of Table 1. According to Table 1, one can find that the value of C-stat/dof in the fitting with CPL-mBB is closer to unity than that in the fitting with the Band function. This indicates that the CPL-mBB with $q = 3$ and $s = 1.2$ can present a better description of the radiation spectrum observed in GRB 220426A compared with the Band function. It reveals that the prompt emission of GRB 220426A originates from the photosphere.

4. Discussion

The identification of the emission from the photosphere allows one to determine the physical properties of the relativistic outflow, such as the bulk Lorentz factor Γ_{ph} and the radius r_{ph} of the photosphere, and the initial size of the flow R_0 (Pe'er et al. 2007). In the case of $r_{ph} > r_s = \Gamma R_0$, the photospheric radius is given by $r_{ph} = P_{jet}\sigma_T / 8\pi\Gamma^3 m_p c^3$, where P_{jet} is the power of the jet. In addition, one can have $P_{jet} = 4\pi d_L^2 (r_{ph}/r_s)^{2/3} F_{ph}$, $T_{ph} = T_0 (r_{ph}/r_s)^{-2/3}$, and $T_0 = [P_{jet}(t) \big/ (16\pi R_0^2 \sigma)]^{1/4}$. Taking Y to represent the radiation efficiency of the jet in the gamma-rays, one can have $P_{jet} = 4\pi d_L^2 Y F_{obs}$, where F_{obs} is the observed spectrally integrated gamma-ray flux and can be estimated as $F_{obs} \simeq F_{ph}$ in GRB 220426A. Then, one can use kT_{ph} and F_{ph} to estimate r_{ph} and Γ_{ph}. In Figure 5, we show the evolution of kT_{ph}, F_{ph}, r_{ph}, Γ_{ph}, and R_0 in the course of the burst. Because the redshift z of GRB 220426A is not known, we take $z = 1$. One can find that the temperature and Lorentz factor of the photosphere decrease with time. However, the radius of the photosphere and the initial size of the flow increase with time. The increase of the Lorentz factor and photospheric radius relative to the time implies that the jet becomes dirtier with time. The increase of R_0 with time may reflect the evolution of the environment for the jet formation.

The time-resolved spectral analysis of GRB 090902B reveals a significant power-law component that is distinct from the main radiation component (Abdo et al. 2009, see also the right panel of Figure 1 in this paper). We also note that there seems to be an additional component in the radiation spectrum of GRB 220426A. Then, we would like to fit the radiation spectrum with CPL-mBB and the power-law spectral model $F(E) = F_0 E^{-\beta}$. The fitting results are shown in the left panel of Figure 6, where the time interval of [1, 2] s is fitted as an example. The best-fitting result reveals that the power-law spectral component

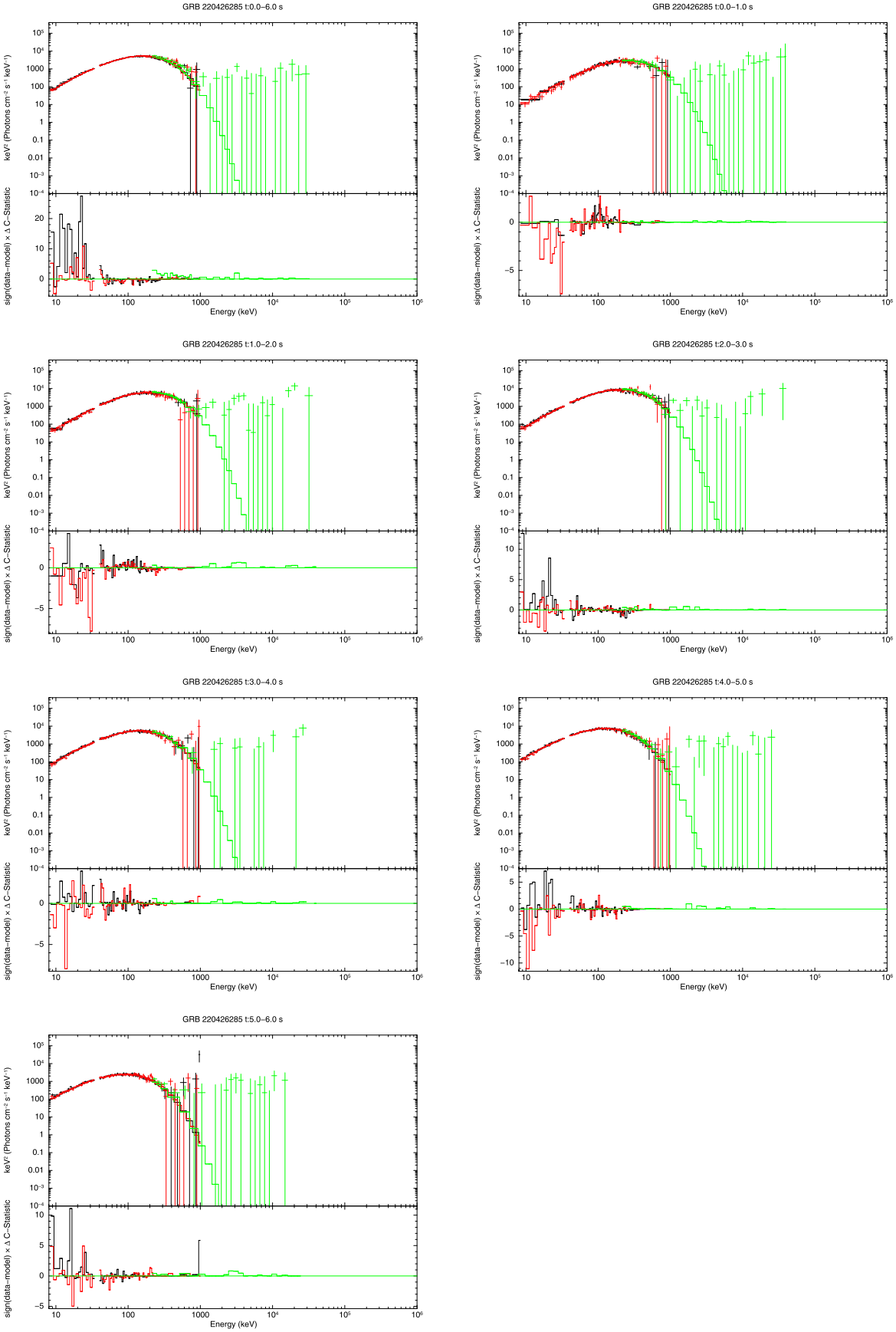

Figure 4. Same as Figure 3, but with the CPL-mBB spectral model in the fittings.

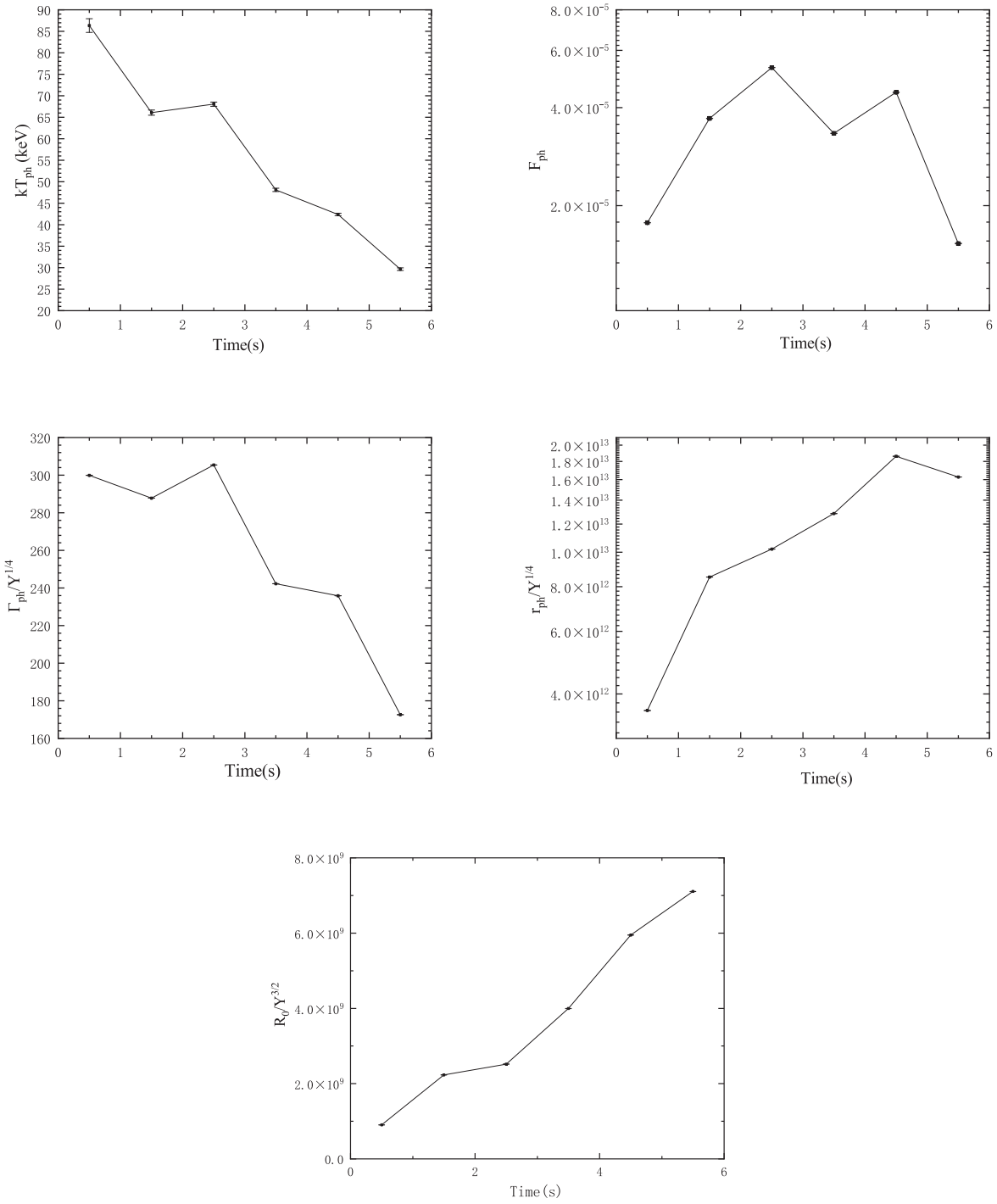

Figure 5. Evolution of $kT_{\rm ph}$, $F_{\rm ph}$, $\Gamma_{\rm ph}$, $r_{\rm ph}$, and R_0 in the course of the burst.

is presented with $\beta \sim -2.01 \pm 1.36$. The power-law spectral model with $\beta \sim -2.01 \pm 1.36$ is very similar to the spectral shape in the low-energy regime of the radiation spectrum in the CPL-mBB model. It may reveal that the high-energy emission in this burst may be formed by the inverse Compton of the CPL-mBB photons by the electrons. Then, we perform the calculation of the inverse Compton of the CPL-mBB photons by the electrons with different γ_e and $\tau_{\rm e} = \sigma_{\rm T} n_{\rm e} = 0.01$, where $\sigma_{\rm T}$ is the Thomson cross section, $n_{\rm e}$ is the number of electrons per square centimeter along the line of sight, and $\Gamma_{\rm ph} = 200$ is adopted. The inverse Compton component can be found in the right panel of Figure 6. One can find that the spectral shape of the inverse Compton component in the high-energy regime can be described with a power-law function $F(E) \propto E^{\sim 1}$, which is slightly different from the reported spectral fitting result but within the error bound. Pe'er et al. (2012) have studied the connection between the thermal component and nonthermal component in GRB 090902B. They argued that the three emission mechanisms, i.e., synchrotron emission, synchrotron self-Compton emission, and Comptonization of the thermal photons, contribute the same order of magnitude to the radiation spectrum above the thermal peak. When the synchrotron and synchrotron self-Compton emission component make a significant contribution to the spectrum above the thermal peak of GRB 220426A,

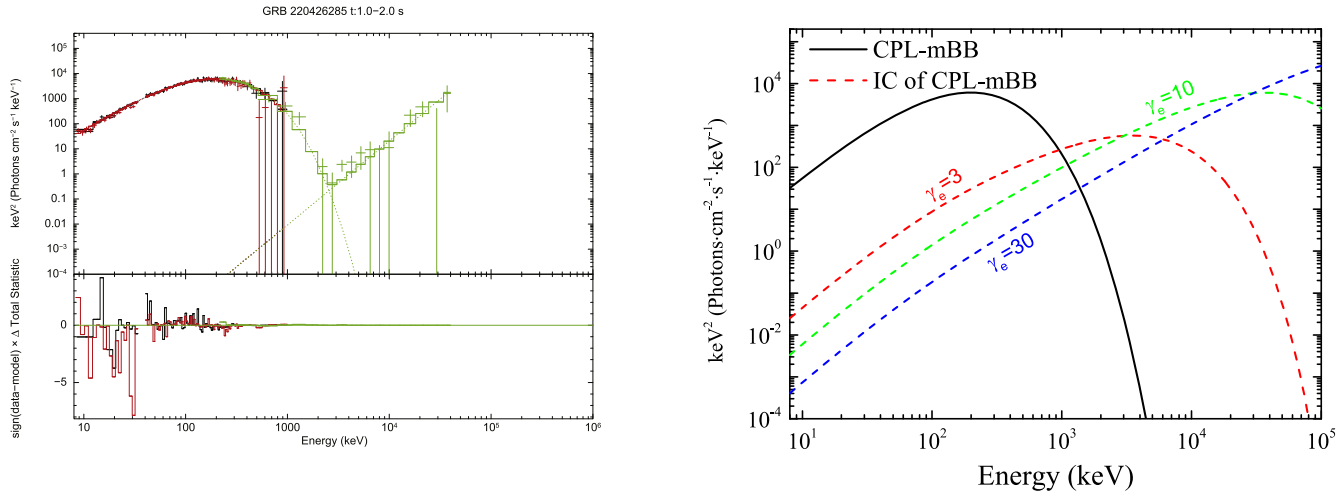

Figure 6. Spectral fitting results with CPL-mBB and the power-law spectral model (left panel) and theoretical inverse Compton spectrum of the CPL-mBB photons (right panel).

however, the spectrum above the thermal peak may be shallower than $F(E) \propto E^{\sim 1}$.

There are also quite a few cases where a thermal component was claimed in the time-integrated or time-resolved radiation spectra but is not dominant in the radiation spectrum (e.g., Guiriec et al. 2011; Axelsson et al. 2012; Guiriec et al. 2013). In these bursts, the thermal component is presented as a "shoulder" of the main radiation component. It suggests that these bursts are in fact different from GRB 090902B and thus GRB 220426A, for which the dominant radiation component is the photospheric emission. Hou et al. (2018) found that the radiation spectra of GRB 081221 can be well fitted with PL-mBB. For this burst, we also perform spectral fittings with the Band function or CPL-mBB. The radiation spectral fittings with the Band function for GRB 081221 generally report low values of $\alpha \sim -0.7$, which implies a broad radiation spectrum compared with those in GRB 220426A and GRB 090902B ($\lesssim$12 s after the burst trigger). It should be pointed out that these kinds of broad radiation spectra could not be well described by CPL-mBB with $q = 3$ and $s = 1.2$. In fact, our spectral fittings reveal that the values of C-stat/dof ($\gtrsim$1.4) reported in the fittings with CPL-mBB, $q = 3$, and $s = 1.2$ for this burst are higher than the values of C-stat/dof ($\sim$1.2) reported in the fittings with Band function. In addition, both GRB 220426A and GRB 090902B have a power-law component that is distinct from the main radiation component. Then, we would like to believe that GRB 220426A would be the second case in the class of GRB 090902B, for which the dominated radiation component can be well modeled with a nondissipated photospheric emission.

5. Conclusion

In this paper, we report on a very bright, long-duration gamma-ray burst, GRB 220426A, observed by the Fermi satellite. With a total duration of $T_{90} = 6$ s, GRB 220426A is composed of two main pulses and some subpeaks. The spectral analysis of this burst reveals a very narrow Band component around 100 keV, which is highly reminiscent of GRB 090902B. Then, we perform a detailed spectral analysis of this burst based on the model of a nondissipated photospheric emission. Here, the emission of a nondissipated photospheric emission is modeled as a multicolor blackbody with a cutoff power-law distribution of the thermal temperature. It is found that the photospheric emission can present a better description of the radiation spectrum of this burst compared with the Band function. We thus conclude that this burst would be the second burst in the class of GRB 090902B observed by the Fermi satellite.

We thank the anonymous referee of this work for useful comments and suggestions that improved the paper. We acknowledge the use of the Fermi archive's public data. This work is supported by the Guangxi Science Foundation (grant Nos. 2018GXNSFFA281010, 2018GXNSFGA281007, and 2018GXNSFDA281033) and the National Natural Science Foundation of China (grant Nos. 11773007, 12133003, U1938116, U1938201, and U1938106).

ORCID iDs

Da-Bin Lin https://orcid.org/0000-0003-1474-293X
Jing Li https://orcid.org/0000-0002-6019-7381
Xiang-Gao Wang https://orcid.org/0000-0001-8411-8011
Rui-Jing Lu https://orcid.org/0000-0003-2467-3608
En-Wei Liang https://orcid.org/0000-0002-7044-733X

References

Abdo, A. A., Ackermann, M., Ajello, M., et al. 2009, ApJL, 706, L138
Axelsson, M., Baldini, L., Barbiellini, G., et al. 2012, ApJL, 757, L31
Beniamini, P., & Giannios, D. 2017, MNRAS, 468, 3202
Biltzinger, B., Kunzweiler, F., Berlato, F., Greiner, J., & Burgess, J. 2022, GCN, 31950, 1
Daigne, F., Bošnjak, Ž., & Dubus, G. 2011, A&A, 526, A110
Daigne, F., & Mochkovitch, R. 2002, MNRAS, 336, 1271
Deng, W., & Zhang, B. 2014, ApJ, 785, 112
Frederiks, D., Lysenko, A., Ridnaia, A., et al. 2022, GCN, 31959, 1
Gao, H., & Zhang, B. 2015, ApJ, 801, 103
Ghirlanda, G., Pescalli, A., & Ghisellini, G. 2013, MNRAS, 432, 3237
Ghisellini, G., & Celotti, A. 1999, ApJL, 511, L93
Giannios, D. 2008, A&A, 480, 305
Guiriec, S., Connaughton, V., Briggs, M. S., et al. 2011, ApJL, 727, L33
Guiriec, S., Daigne, F., Hascoët, R., et al. 2013, ApJ, 770, 32
Hou, S.-J., Zhang, B.-B., Meng, Y.-Z., et al. 2018, ApJ, 866, 13
Larsson, J., Racusin, J. L., & Burgess, J. M. 2015, ApJL, 800, L34
Lazzati, D., & Begelman, M. C. 2010, ApJ, 725, 1137
Lazzati, D., Morsony, B. J., Margutti, R., & Begelman, M. C. 2013, ApJ, 765, 103
Lloyd, N. M., & Petrosian, V. 2000, ApJ, 543, 722

Malacaria, C., Meegan, C., & Fermi, G. B. M. 2022, GCN, 31955, 1
Meegan, C., Lichti, G., Bhat, P. N., et al. 2009, ApJ, 702, 791
Mészáros, P., Ramirez-Ruiz, E., Rees, M. J., & Zhang, B. 2002, ApJ, 578, 812
Mészáros, P., & Rees, M. J. 2000, ApJ, 530, 292
Mizuta, A., Nagataki, S., & Aoi, J. 2011, ApJ, 732, 26
Pe'er, A. 2008, ApJ, 682, 463
Pe'er, A., Mészáros, P., & Rees, M. J. 2006, ApJ, 642, 995
Pe'er, A., Ryde, F., Wijers, R. A. M. J., Mészáros, P., & Rees, M. J. 2007, ApJL, 664, L1
Pe'er, A., Zhang, B. B., Ryde, F., et al. 2012, MNRAS, 420, 468
Preece, R. D., Briggs, M. S., Mallozzi, R. S., et al. 2000, ApJS, 126, 19
Rees, M. J., & Mészáros, P. 2005, ApJ, 628, 847
Ruffini, R., Siutsou, I. A., & Vereshchagin, G. V. 2013, ApJ, 772, 11
Ryde, F. 2004, ApJ, 614, 827
Ryde, F. 2005, ApJL, 625, L95
Ryde, F., Axelsson, M., Zhang, B. B., et al. 2010, ApJL, 709, L172
Ryde, F., & Pe'er, A. 2009, ApJ, 702, 1211
Tavani, M. 1996, ApJ, 466, 768
Thompson, C. 1994, MNRAS, 270, 480
Thompson, C., Mészáros, P., & Rees, M. J. 2007, ApJ, 666, 1012
Toma, K., Wu, X.-F., & Mészáros, P. 2011, MNRAS, 415, 1663
Uhm, Z. L., & Zhang, B. 2014, NatPh, 10, 351
Zhang, B., & Mészáros, P. 2002, ApJ, 581, 1236
Zhang, B., & Yan, H. 2011, ApJ, 726, 90
Zhang, B.-B., Zhang, B., Liang, E.-W., et al. 2011, ApJ, 730, 141